N O T I C E

THIS DOCUMENT HAS BEEN REPRODUCED FROM MICROFICHE. ALTHOUGH IT IS RECOGNIZED THAT CERTAIN PORTIONS ARE ILLEGIBLE, IT IS BEING RELEASED IN THE INTEREST OF MAKING AVAILABLE AS MUCH INFORMATION AS POSSIBLE

Shockless Design and Analysis of Transonic Blade Shapes

Djordje S. Dulikravich
Lewis Research Center
Cleveland, Ohio
and
Helmut Sobieczky
DFVLR — Institute für Theoretische Strömungsmechanik
Göttingen, Federal Republic of Germany

NASA

SHOCKLESS DESIGN AND ANALYSIS OF TRANSONIC BLADE SHAPES

Djordje S. Dulikravich*
National Aeronautics and Space Administration
Lewis Research Center
Cleveland, Ohio 44135

and

Helmut Sobieczky**
DFVLR-Institut für
Theoretische Strömungsmechanik
Göttingen, Federal Republic of Germany

Abstract

A fast computer program has been developed that can be used in two basic modes: (1) an analysis mode for steady, transonic, potential flow through a given planar cascade of airfoils and (2) a design mode for converting a given cascade into a shockless transonic cascade. The design mode can automatically be followed by the analysis mode, thus confirming that the new flow field found is shock free. The program generates its own multilevel boundary-conforming computational grids and solves a full-potential equation in a fully conservative form. The shockless design is performed by implementing Sobieczky's fictitious-gas elliptic continuation concept.

Nomenclature

a	speed of sound (isentropic)
a_*	speed of sound (critical
a_f	speed of sound (fictitious)
C_D	coefficient of aerodynamic drag force (x direction)
C_L	coefficient of aerodynamic lift force (y direction)
c	airfoil chord length
D	determinant: $a(x,y)/a(X,Y)$
g	y-distance between corresponding points on neighboring airfoils
M	local Mach number ($M = q/a$)
M_*	critical Mach number ($M_* = q/a_*$)
M_1	Mach number at upstream infinity
M_2	Mach number at downstream infinity
m	coordinate direction orthogonal to streamline
P	constant in fictitious-gas relation
q	magnitude of local velocity vector
S	entropy
U, V	contravariant components of velocity vector in (X,Y) plane
u, v	components of velocity vector in (x,y) plane
x, y	Cartesian coordinates in physical plane
X, Y	Cartesian coordinates in computational plane
α_1, α_2	free-stream angles at upstream and downstream infinity
β	cascade stagger angle
γ	ratio of specific heats
θ	angle between x axis and velocity vector
ν	Prandtl-Meyer function

ρ	isentropic fluid density
ρ_*	critical fluid density
ρ_f	fictitious fluid density
ϕ	velocity vector potential ($\vec{\nabla}\phi = \vec{q}$)
ψ	stream function

*Visiting Research Scientist presently employed by the Universities Space Research Association. Member AIAA.
**Research Scientist. Member AIAA.

Introduction

In the general case of transonic cascade flow, supersonic regions terminate with shocks. These shocks create vorticity and generate entropy in a flow field that was initially irrotational and homentropic. As a consequence the aerodynamic drag force sharply increases (wave drag) and the total energy decreases, resulting in a rapid decay of the aerodynamic efficiency of the cascade and an abrupt increase in the aerodynamic noise level. In many experiments it has been observed that, if the Mach number just ahead of the foot of the shock wave is larger than approximately 1.3, the boundary layer starts to separate, leading to complex and potentially dangerous unsteady flow phenomena and mechanical vibrations.

Choked flow represents yet another undesirable phenomenon associated with transonic cascade flow. Choking places an upper limit on the mass flow through a given cascade. As a countermeasure the airfoils in the cascade are often positioned farther apart, decreasing cascade solidity. This results in a decrease in flow turning angle through the cascade and a drop in pressure rise across the cascade.

The main objective of this work is therefore to eliminate the shocks (and possibly even the choked flow) by slightly altering portions of the contour of a given airfoil in the cascade.

Analysis

Governing Equations

This work is based on the fictitious-gas concept of Sobieczky[1] and the full-potential, steady, transonic turbomachinery analysis codes of Dulikravich.[2] The analysis was derived extensively in earlier works[3,4] and will be repeated here in its concise form only.

In the case of a steady, two-dimensional, irrotational isentropic flow of an inviscid, compressible fluid the conservative form of the continuity equation is

$$(\rho u)_{,x} + (\rho v)_{,y} = 0 \qquad (1)$$

Equation (1) can also be expressed in its nonconservative full-potential form

$$\rho\left(\left(1 - \frac{\phi_{,x}^2}{a^2}\right)\phi_{,xx} - 2\frac{\phi_{,x}\phi_{,y}}{a^2}\phi_{,xy} + \left(1 - \frac{\phi_{,y}^2}{a^2}\right)\phi_{,yy}\right) = 0$$

$$(2)$$

or in its canonical operator form[5,2]

$$\left(\rho(1 - M^2)\phi_{,ss}^H - \rho(1 - M^2)\phi_{,ss}^E\right) + \rho\left(\nabla^2\phi^E - M^2\phi_{,ss}^E\right) = 0$$

$$(3)$$

Equation (3) represents a quasi-linear, second-order partial differential equation of mixed elliptic-hyperbolic type that accepts isentropic discontinuities in its solution. These isentropic shocks satisfy mass conservation

$$M_{\ast a}M_{\ast b} = M_{\ast b}^2(\rho_a/\rho_b) \qquad (4)$$

and differ from the Rankine-Hugoniot shocks (Table I). Superscript H in equation (3) designates upstream differencing, and superscript E designates central differencing to be used for the evaluation of particular second derivatives. Solution of this steady-state equation is obtained as an asymptotic solution to an artificially unsteady[6] equation

$$\rho\left((1 - M^2)\phi_{,ss} + \phi_{,mm} + 2\xi\phi_{,st} + 2n\phi_{,mt} + \epsilon\phi_{,t}\right) = 0$$

$$(5)$$

for large times, where ξ, n, and ϵ are coefficients. This equation is solved by using an iterative line overrelaxation where consecutive iteration sweeps through the flow field are considered as steps in an artificial time direction. The steady part of the residual (or error) of equation (5) is always evaluated by using equation (1) supplemented by a directional numerical viscosity in a continuously fully conservative form, thus uniquely capturing possible isentropic shocks.

For the purpose of a type-dependent,[7] rotated[5] finite difference evaluation of the derivatives in equation (3) and a finite area[8] evaluation of the first derivatives in equation (1), the flow field and the governing equations are transformed from the physical (x,y) plane (Fig. 1) into a rectangular (X,Y) computational domain (Fig. 2) by using local isoparametric bilinear mapping functions.

If the geometric transformation matrix is

$$[J]^T = \begin{bmatrix} x_{,X} & y_{,X} \\ x_{,Y} & y_{,Y} \end{bmatrix} \qquad (6)$$

then the contravariant velocity components in the (X,Y) plane are

$$\begin{Bmatrix} U \\ V \end{Bmatrix} = [J]^{-1}\begin{Bmatrix} u \\ v \end{Bmatrix} = [J]^{-1}[J^T]^{-1}\begin{Bmatrix} \phi_{,X} \\ \phi_{,Y} \end{Bmatrix} \qquad (7)$$

Consequently the fully conservative form of the continuity equation (eq. (1)) becomes

$$\frac{1}{D}\left((\rho UD + \delta_X)_{,X} + (\rho VD + \delta_Y)_{,Y}\right) = 0 \qquad (8)$$

where the artificial viscosity terms δ_X, δ_Y represent principal parts of a truncation error of equation (3).

The computational grid in the x,y plane is generated by using a sequence of simple geometric transformations[9,10] incorporating a single conformal-mapping function, elliptic polar coordinates, and nonorthogonal coordinate stretching and shearing. The uniform grid (Fig. 2) in the computational (X,Y) plane thus remaps back into the body-fitted, quasi-orthogonal grid of figure 3 in the physical (x,y) plane. The iterative solution process of equation (3) is accelerated by using a four-level, consecutive-grid refinement procedure.

All the flow parameters are nondimensionalized with respect to the critical conditions denoted by an asterisk so that the isentropic relations used for the local fluid density and the speed of sound are[11]

$$\frac{\rho}{\rho_\ast} = \left(\frac{\gamma + 1}{2} - \frac{\gamma - 1}{2}M_\ast^2\right)^{1/(\gamma-1)} \qquad (9)$$

$$\frac{a^2}{a_\ast^2} = \left(\frac{\rho}{\rho_\ast}\right)^{\gamma-1} \qquad (10)$$

Shock-Free Surface Design

Within the last decade several versions of an indirect (hodograph) design approach based on Garabedian's method of complex characteristics have been published.[12] The method proved to be a powerful tool for the design of high-performance airfoils and cascades, but handling the complicated boundary and initial-value problems in a four-dimensional computational space for practically interesting design cases requires a large amount of experience. It is therefore desirable to develop efficient direct - or nearly direct-design methods.

This task can be accomplished by prescribing a smooth, shock-free pressure distribution along a portion of a given airfoil contour in a cascade and then determining a partially new airfoil shape consistent with the prescribed surface flow conditions. Because of the highly nonlinear character of the transonic flow this design technique generally does not provide an entirely shock-free flow field. In order to completely eliminate all shocks (and the associated wave drag) from the flow field, a number of such designs must be performed, and an optimization technique must be devised to search for a cascade that maintains an entirely shock-free flow field for a specific set of flow parameters.

Shock-Free Flow Field Design

Shock-free, or shockless, flow means that the fluid decelerates from a supersonic speed to a subsonic speed not discontinuously (shocked flow), but smoothly over a finite distance (isentropic recompression). This requires determination of a modi-

fied supersonic region that is longer but flatter and thus can possibly unchoke a flow that was originally choked. The sonic line bounding such a supersonic region in an otherwise subsonic flow field must not have inflection points if shocks are to be avoided.

To eliminate the possibility of obtaining shocks anywhere in the flow field, Sobieczky proposed[1] and successfully applied[13,14] the concept of a fictitious-gas, shock-free design that corresponds to an elliptic continuation[3] from the subsonic flow into local supersonic flow domains. This design technique uses isentropic relations for fluid density (eq. (9)) and the sound speed (eq. (10)) only where the flow is locally subsonic. At every point where the flow is locally supersonic, modified (artificial) relations are used for the fluid density and the sound speed so that the governing equation remains elliptic throughout the flow field. Therefore any conservative computer code capable of solving a subcritical potential flow field can be modified to include the fictitious gas concept and then serve as a tool for determining the sonic line shape.

It is important to point out[14] that the flow field outside the supersonic bubble calculated from the fictitious-gas relations is already the correct subsonic flow field. It is only the supersonic part of the flow field that must be recomputed and from this recalculation a new portion of the shock-free airfoil surface determined. Lift and drag coefficients are also already design results, and they will not be altered by the subsequent recomputation of the local supersonic region. The sole purpose of originally using an fictitious gas (modified density and sound speed relation) is thus to determine a shape of the sonic line that is compatible with an entirely shock-free flow field.

In the two-dimensional case of a cascade of airfoils the values of potential ϕ and stream function ψ on the sonic line obtained from the fictitious-gas calculation serve as the initial data for an integration by the method of characteristics. This integration is performed in a triangle ERC of a rheograph (Fig. 4) plane (local flow angle θ versus Prandtl-Meyer function $\nu(M_*)$. This recalculation (now using isentropic gas relations (eq. (9) and Eq. (10)) is performed only inside the supersonic flow domain. The new section of the airfoil surface is then determined from the arc $\psi = 0$, which is interpolated from the solution in the characteristic triangle ERC (Fig. 4). The new airfoil is slightly flatter than the original shape: Isentropic flow requires more space to pass than the fictitious one.

The fictitious-gas technique is not limited in application only to two-dimensional planar problems like a hodograph technique; it can be successfully applied to both arbitrary two-dimensional and three-dimensional[13,14] configurations.

Fictitious-Gas Relations

The fictitious-gas relation ρ_f/ρ_* is applied only in the regions where $M > 1$. An arbitrary analytic expression for ρ_f/ρ_* is nevertheless subject to several constraints (Fig. 5). It should satisfy the first-order continuity condition on the sonic line in the flow field; that is,

$$\frac{d}{dM_*}\left(\frac{\rho_f}{\rho_*}\right) = -1 \qquad (11)$$

when $M = 1$. It is desirable to use a formula for ρ_f/ρ_* that includes a single (preferably constant) input parameter P that makes the fictitious gas more or less compressible in the supersonic regions. Such a function must not have minimum or maximum values in the range of expected relative local Mach numbers, because at such points the local fictitious speed of sound a_f/a_* is infinite. This can be observed if the general continuity criterion

$$\frac{\rho_f}{\rho_*} = \exp\left(-\int_{a_*}^{q} \frac{q\,dq}{a_f^2}\right) \qquad (12)$$

is used to obtain the relation for a_f/a_*. After taking a logarithm and a derivative of both sides of equation (12) one gets a general expression for the speed of sound of the fictitious gas

$$\frac{a_f^2}{a_*^2} = -M_* \frac{\rho_f}{\rho_*} \frac{1}{\dfrac{d}{dM_*}\left(\dfrac{\rho_f}{\rho_*}\right)} \qquad (13)$$

For the purpose of guaranteeing an entirely shock-free flow field the values for ρ_f/ρ_* must always be higher than the values required by the parabolicity condition; that is, $(\rho_f/\rho_*) = M_*^{-1}$ (Fig. 5). The final condition for the relation $\rho_f/\rho_* = F(M_*; P)$ is that it should be a very simple function that will also produce a simple expression for a_f/a_*.

In the present work we use the relation

$$\frac{\rho_f}{\rho_*} = 1 + \frac{1 - \sqrt{1 + 4P(M_* - 1)}}{2P} \qquad (14)$$

which gives

$$\frac{a_f^2}{a_*^2} = M_*\left(1 + \frac{1 - \sqrt{1 + 4P(M_* - 1)}}{2P}\right)\sqrt{1 + 4P(M_* - 1)} \qquad (15)$$

Results

Based on the preceding analysis, computer code[15] DCAS2D has been developed and tested for the following sequence of test cases. For the purpose of illustrating basic features of the flow through planar cascades of airfoils the flow around an isolated NACA 0012 airfoil in free air and the flow through a cascade of NACA 0012 airfoils were analyzed. Airfoils in the cascade had zero stagger angle ($\beta = 0°$) and a gap-chord ratio of 3.6 ($g/c = 3.6$). The free-stream angle was zero at both upstream and downstream infinity. In the case of an incompressible free stream ($M_1 = 0.001$) the result obtained for the cascade did not differ from the result obtained for an isolated airfoil.[2] But in

3

the case of a transonic flow ($M_1 = 0.8$) the cascade effects (Fig. 6) were very significant even for such widely spaced airfoils.

To demonstrate the applicability of shock-free, fictitious-gas design to realistic lifting, staggered cascades, we use a simple analytical shape generator for geometry definition of the input airfoils. Flexible geometry definition is most useful for parametric studies of cascades. Here we use a formula for blade section definition:

$$y = Ax + Bx^C + x^{1/2}(1 - x)^{1/2} \left(D + Ex + Fx(1 - x) \right)$$

(16)

with a proper choice of the parameters to control leading- and trailing-edge radii, angles, and thickness distribution.

Figure 7 shows a cascade of this family, with a sonic line and the corresponding modification on the upper surface, where shock-free redesign[15] for chosen operating conditions flattened the airfoil contour. For this cascade the global flow and geometric parameters were $M_1 = 0.8$, $g/c = 0.85$, $\alpha_1 = 41°$, $\alpha_2 = 17°$, and $\beta = 27.3°$.

It is shown in Figure 8 that the airflow through this cascade with geometry given by equation (16) and a gap-chord ratio of 0.85 is not shock-free but contains a very strong shock. For the same global flow conditions the design mode of the code DCAS2D is then used to obtain a new shape (Fig. 7). This shape is different from the initial airfoil only between 3 and 38 percent of chord on the upper surface, resulting in a shock-free (Fig. 9) pressure distribution. Then the analysis mode of DCA2SD is used to verify that the design flow agreement is excellent (Fig. 10).

This is the first of a series of examples from a parametric cascade airfoil shape study.[16] Although the new airfoil losses shock-free properties at off-design conditions (Fig. 11), the resulting shock is still considerably weaker than a shock on the original airfoil. An optimum cascade for a range of operating conditions can be obtained by combining the fictitious-gas design concept with an optimization technique.

As already mentioned, computer code DCAS2D is capable of converting a choked, shocked cascade flow field into an unchoked, shock-free flow field. To illustrate this feature we selected a non-staggered cascade of NACA 0018 airfoils having a gap-chord ratio g/c of 1. Note that a simple one-dimensional[11] flow assumption predicts that the flow through this cascade will choke if $M_1 > 0.577$. Therefore we used the design mode of the DCAS2D code with $M_1 = 0.582$ and the fictitious-gas parameter $\bar{P} = 500$. The resulting flow field (Fig. 12) is unchoked and entirely shock free.

All the calculations were performed without taking into account viscous boundary layer effects. For this purpose one may use a standard boundary layer calculation procedure because shock - boundary layer interaction effects do not exist in a shock-free flow. The viscous/inviscid calculation can be performed iteratively with a treatment of trailing-edge viscous interaction, as has been demonstrated[17] for isolated supercritical airfoils.

Concluding Remarks

An efficient and reliable computer program, DCAS2D, has been developed and tested that automatically performs partial redesign of a given airfoil shape in the cascade for the purpose of eliminating shock waves and the associated wave drag. The code represents an application of already known and successfully applied numerical techniques for transonic flow analysis and the shock-free flow field design. These techniques are based on the finite volume and a fictitious-gas approach, respectively. A new formula for the fictitious-gas relation, accompanied with the related physical constraints, has been suggested.

The computer code is entirely self-sufficient in generating its own multilevel boundary-conforming grids. The code can operate separately as a shock-free cascade design code and also as a general transonic cascade analysis program with the capability to accurately capture isentropic shocks.

Acknowledgment

References

1. Sobieczky, H., "Transonic Fluid Dynamics - Lecture Notes," The University of Arizona, TFD 77-01, Oct. 1977.
2. Dulikravich, D. S., "CAS2D - Fortran Program for Nonrotating Blade-to-Blade, Steady, Potential Transonic Cascade Flows," NASA TP-1705, 1980.
3. Sobieczky, H., "Rheograph Transformation and Continuation Methods," in Mathematical Methods in Fluid Mechanics, Von Karman Institute for Fluid Dynamics, VKI-LS-1980-4, Feb. 1980.
4. Dulikravich, D. S., "Numerical Calculation of Inviscid Transonic Flow Through Rotors and Fans," Ph.D. Thesis, Cornell Univ., 1979. Avail. Univ. Microfilms, Order No. 79.0741, 300 N. Zeeb Rd., Ann Arbor, MI, 48106.
5. Jameson, A., "Transonic Flow Calculations," in Computational Fluid Dynamics, Vol. 1, Von Karman Institute, VKI-LS-87-VOL-1, 1976, pp. 1.1-5.84.
6. Garabedian, P., "Estimation of the Relaxation Factor for Mesh Sizes," Math. Tables Aids to Comput., Vol. 10, 1956, 183-185.
7. Murman, E. M., and Cole, J., "Calculation of Plane Steady Transonic Flows," AIAA Journal, Vol. 9, 1971, pp. 114-121.
8. Jameson, A., and Caughey, D., "A Finite Volume Scheme for Transonic Potential Flow Calculations," AIAA 3rd Computational Fluid Dynamics Conference, 1977, Paper 77-635, pp. 35-54.
9. Dulikravich, D. S., and Caughey, D. A., "Finite Volume Calculation of Transonic Potential Flow Through Rotors and Fans," FDA-80-03, Cornell University, 1980.

10. Dulikravich, D. S., "Numerical Calculation of Transonic Axial Turbomachinery Flows," 7th International Conference on Numerical Methods in Fluid Mechanics, Stanford University, Stanford, Calif., June 23-27, 1980. (also NASA TM 81544, 1980.)

11. "Equations, Tables and Charts for Compressible Flow," NACA TR-1135, 1953.

12. Garabedian, P. R., and Korn, D. G., "Numerical Design of Transonic Airfoils," Numerical Solution to Partial Differential Equations, Vol. II-SYNSPADE 1970, Academic Press, New York, 1978, pp. 253-271.

13. Sobieczky, H., Fung, K-Y., Yu, N. and Seebass, R., "A New Method for Designing Shock-free Transonic Configurations," AIAA Journal, Vol. 17, no. 7, July 1979, pp. 722-729.

14. Sobieczky, H., "Design of Advanced Technology Transonic Airfoils and Wings," Subsonic/Transonic Configuration Aerodynamics, AGARD Fluid Dynamics Panel Symposium, AGARD CP-285, 1980.

15. Dulikravich, D. S., "DCAS2D - Computer Program for Fast Design and Analysis of Shock Free Airfoil Cascades," to be published as NASA TP, 1981.

16. Sobieczky, H., Dulikravich, D. S., "Design Examples for Supercritical Cascades," to be published as DFVLR report, 1981.

17. Nebeck, H. E., Seebass, A. R., and Sobieczky, H., "Inviscid-Viscous Interactions in the Nearly-Direct Design of Shock-Free Supercritical Airfoils," Presented at AGARD FDP Symposium on Computation of Viscous/Inviscid Interaction, 1980.

TABLE I. RANKINE-HUGONIOT ($\overline{M}_b*$) AND ISENTROPIC (M_b*, M_b) SHOCK JUMP RELATIONS

| M_a*	$\overline{M}_b*$	M_b*	M_a	M_b
1.00500	0.99502	0.99500	1.00601	0.99401
1.01000	0.99010	0.99001	1.01204	0.98804
1.01500	0.98522	0.98502	1.01808	0.98210
1.02000	0.98039	0.98003	1.02415	0.97617
1.02500	0.97561	0.97504	1.03023	0.97027
1.03000	0.97087	0.97006	1.03633	0.96439
1.03500	0.96618	0.96508	1.04245	0.95853
1.04000	0.96154	0.96011	1.04859	0.95269
1.04500	0.95694	0.95514	1.05475	0.94687
1.05000	0.95238	0.95017	1.06093	0.94107
1.05500	0.94787	0.94520	1.06713	0.93529
1.06000	0.94340	0.94024	1.07335	0.92952
1.06500	0.93897	0.93528	1.07959	0.92378
1.07000	0.93458	0.93033	1.08585	0.91806
1.07500	0.93023	0.92538	1.09213	0.91236
1.08000	0.92593	0.92043	1.09843	0.90668
1.08500	0.92166	0.91548	1.10476	0.90101
1.09000	0.91743	0.91054	1.11110	0.89537
1.09500	0.91324	0.90560	1.11747	0.88974
1.10000	0.90909	0.90067	1.12385	0.88413
1.10500	0.90498	0.89574	1.13026	0.87854
1.11000	0.90090	0.89081	1.13670	0.87297
1.11500	0.89686	0.88589	1.14315	0.86741
1.12000	0.89286	0.88096	1.14963	0.86188
1.12500	0.88889	0.87605	1.15613	0.85636
1.13000	0.88496	0.87113	1.16265	0.85086
1.13500	0.88106	0.86622	1.16920	0.84538
1.14000	0.87719	0.86132	1.17577	0.83991
1.14500	0.87336	0.85641	1.18236	0.83446
1.15000	0.86957	0.85151	1.18898	0.82903
1.15500	0.86580	0.84662	1.19563	0.82361
1.16000	0.86207	0.84173	1.20229	0.81821
1.16500	0.85837	0.83684	1.20899	0.81283
1.17000	0.85470	0.83195	1.21571	0.80747
1.17500	0.85106	0.82707	1.22245	0.80212
1.18000	0.84746	0.82219	1.22922	0.79678
1.18500	0.84388	0.81732	1.23602	0.79147
1.19000	0.84034	0.81245	1.24284	0.78617
1.19500	0.83682	0.80759	1.24969	0.78088
1.20000	0.83333	0.80272	1.25656	0.77561
1.20500	0.82988	0.79787	1.26346	0.77036
1.21000	0.82645	0.79301	1.27039	0.76512
1.21500	0.82305	0.78816	1.27735	0.75990
1.22000	0.81967	0.78331	1.28434	0.75469
1.22500	0.81633	0.77847	1.29135	0.74950
1.23000	0.81301	0.77363	1.29840	0.74433
1.23500	0.80972	0.76880	1.30547	0.73917
1.24000	0.80645	0.76397	1.31257	0.73402
1.24500	0.80321	0.75914	1.31970	0.72889
1.25000	0.80000	0.75432	1.32686	0.72377
1.25500	0.79681	0.74950	1.33405	0.71867
1.26000	0.79365	0.74469	1.34128	0.71358
1.26500	0.79051	0.73988	1.34853	0.70851
1.27000	0.78740	0.73508	1.35581	0.70345
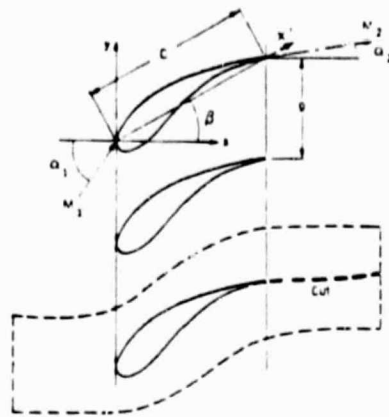
Figure 1. - Planar cascade of airfoils in physical (x, y) plane.
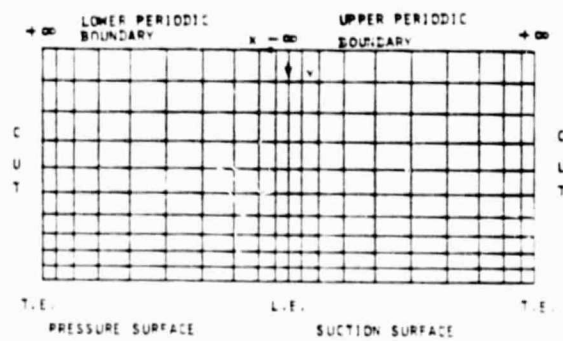

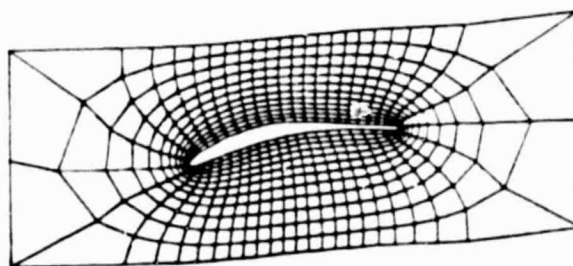Figure 2. - Periodic flow field in (X, Y) computational plane.

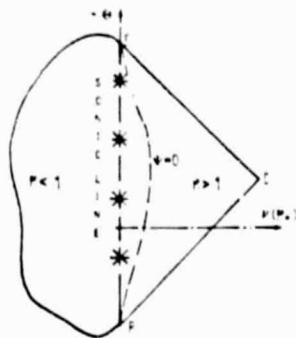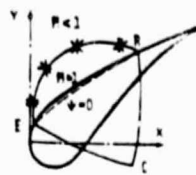Figure 3. - Computational grid in physical (x, y) plane.
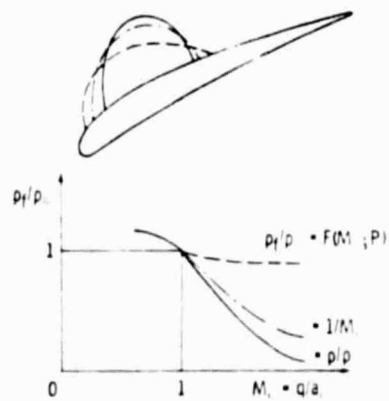
Figure 4. - Physical versus rheograph plane.

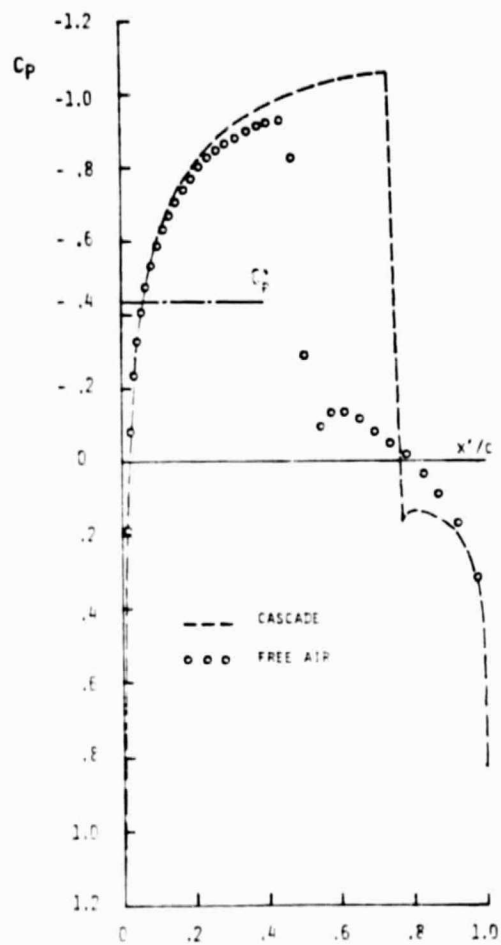
Figure 5. - Sonic line shapes for various density relations.

Figure 6. - Transonic cascade effects. (Airfoil, NACA 0012; $M_1 = M_2 = 0.8$; $g/c = 3.6$; $\alpha_1 = \alpha_2 = \beta = 0°$.)
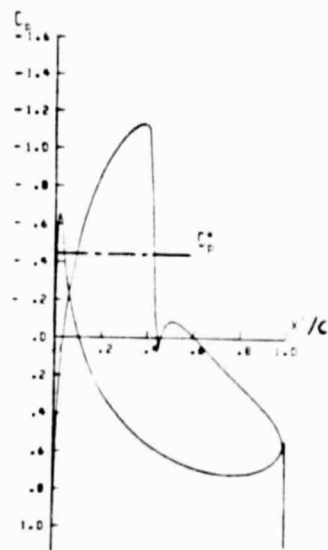
Figure 7. - Original and shock-free cascade of airfoils.

Figure 8. - Original analysis of a given cascade (M_1 = 0.8; g/c = 0.85; α_1 = 41°; α_2 = 17°; β = 27.3°).
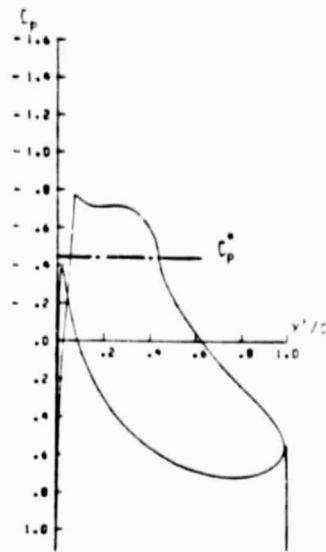
Figure 9. - Shock-free redesign
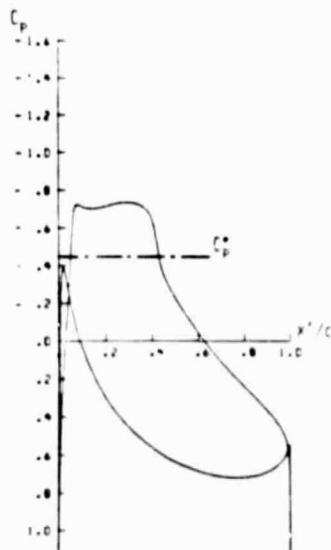of a given cascade (with P = 25
in eqs. (14) and (15)).

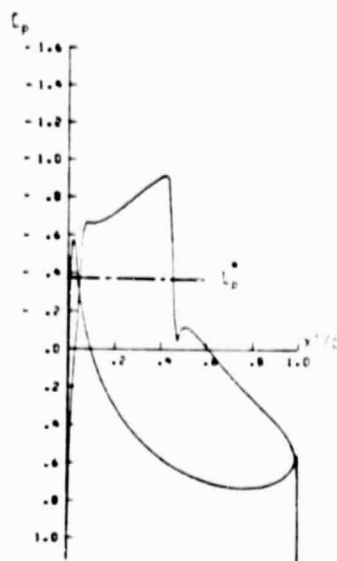Figure 10. - Analytical verifi-
cation of a shock-free design.

Figure 11. - Analysis of shock-
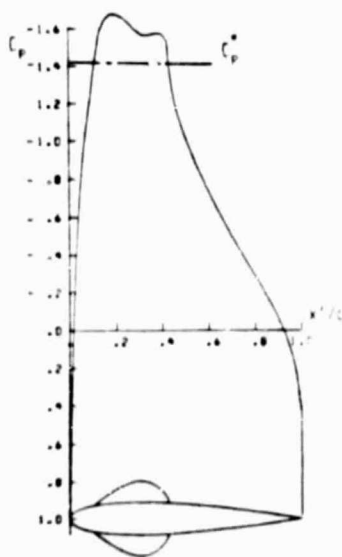free airfoil at an off-design
condition (M_1 • 0.82).

Figure 12. - Unchoking a choked
cascade flow (airfoil, NACA
0018; M_1 • M_2 • 0.582; a_1 •
a_2 • B • 0°; g/c • 1; P • 5.0).